arXiv:hep-ex/0603014v1 7 Mar 2006

Photoproduction of Dijets with High Transverse Momenta at HERA

H1 Collaboration

Abstract

Differential dijet cross sections are measured in photoproduction in the region of photon virtualities $Q^2 < 1\,\text{GeV}^2$ with the H1 detector at the HERA ep collider using an integrated luminosity of $66.6\,\text{pb}^{-1}$. Jets are defined with the inclusive $k_\perp$ algorithm and a minimum transverse momentum of the leading jet of $25\,\text{GeV}$ is required. Dijet cross sections are measured in direct and resolved photon enhanced regions separately. Longitudinal proton momentum fractions up to 0.7 are reached. The data compare well with predictions from Monte Carlo event generators based on leading order QCD and parton showers and with next-to-leading order QCD calculations corrected for hadronisation effects.

A. Aktas[9], V. Andreev[25], T. Anthonis[3], B. Antunovic[26], S. Aplin[9], A. Asmone[33], A. Astvatsatourov[3], A. Babaev[24], S. Backovic[30], J. Bähr[38], A. Baghdasaryan[37], P. Baranov[25], E. Barrelet[29], W. Bartel[9], S. Baudrand[27], S. Baumgartner[39], J. Becker[40], M. Beckingham[9], O. Behnke[12], O. Behrendt[6], A. Belousov[25], Ch. Berger[1], N. Berger[39], J.C. Bizot[27], M.-O. Boenig[6], V. Boudry[28], J. Bracinik[26], G. Brandt[12], V. Brisson[27], D. Bruncko[15], F.W. Büsser[10], A. Bunyatyan[11,37], G. Buschhorn[26], L. Bystritskaya[24], A.J. Campbell[9], F. Cassol-Brunner[21], K. Cerny[32], V. Cerny[15,46], V. Chekelian[26], J.G. Contreras[22], J.A. Coughlan[4], B.E. Cox[20], G. Cozzika[8], J. Cvach[31], J.B. Dainton[17], W.D. Dau[14], K. Daum[36,42], Y. de Boer[24], B. Delcourt[27], M. Del Degan[39], A. De Roeck[9,44], K. Desch[10], E.A. De Wolf[3], C. Diaconu[21], V. Dodonov[11], A. Dubak[30,45], G. Eckerlin[9], V. Efremenko[24], S. Egli[35], R. Eichler[35], F. Eisele[12], E. Elsen[9], W. Erdmann[39], S. Essenov[24], A. Falkewicz[5], P.J.W. Faulkner[2], L. Favart[3], A. Fedotov[24], R. Felst[9], J. Feltesse[8], J. Ferencei[15], L. Finke[10], M. Fleischer[9], P. Fleischmann[9], G. Flucke[33], A. Fomenko[25], I. Foresti[40], G. Franke[9], T. Frisson[28], E. Gabathuler[17], E. Garutti[9], J. Gayler[9], C. Gerlich[12], S. Ghazaryan[37], S. Ginzburgskaya[24], A. Glazov[9], I. Glushkov[38], L. Goerlich[5], M. Goettlich[9], N. Gogitidze[25], S. Gorbounov[38], C. Goyon[21], C. Grab[39], T. Greenshaw[17], M. Gregori[18], B.R. Grell[9], G. Grindhammer[26], C. Gwilliam[20], D. Haidt[9], L. Hajduk[5], M. Hansson[19], G. Heinzelmann[10], R.C.W. Henderson[16], H. Henschel[38], G. Herrera[23], M. Hildebrandt[35], K.H. Hiller[38], D. Hoffmann[21], R. Horisberger[35], A. Hovhannisyan[37], T. Hreus[15], S. Hussain[18], M. Ibbotson[20], M. Ismail[20], M. Jacquet[27], L. Janauschek[26], X. Janssen[9], V. Jemanov[10], L. Jönsson[19], D.P. Johnson[3], A.W. Jung[13], H. Jung[19,9], M. Kapichine[7], J. Katzy[9], I.R. Kenyon[2], C. Kiesling[26], M. Klein[38], C. Kleinwort[9], T. Klimkovich[9], T. Kluge[9], G. Knies[9], A. Knutsson[19], V. Korbel[9], P. Kostka[38], K. Krastev[9], J. Kretzschmar[38], A. Kropivnitskaya[24], K. Krüger[13], J. Kückens[9], M.P.J. Landon[18], W. Lange[38], T. Laštovička[38,32], G. Laštovička-Medin[30], P. Laycock[17], A. Lebedev[25], G. Leibenguth[39], V. Lendermann[13], S. Levonian[9], L. Lindfeld[40], K. Lipka[38], A. Liptaj[26], B. List[39], J. List[10], E. Lobodzinska[38,5], N. Loktionova[25], R. Lopez-Fernandez[23], V. Lubimov[24], A.-I. Lucaci-Timoce[9], H. Lueders[10], D. Lüke[6,9], T. Lux[10], L. Lytkin[11], A. Makankine[7], N. Malden[20], E. Malinovski[25], S. Mangano[39], P. Marage[3], R. Marshall[20], M. Martisikova[9], H.-U. Martyn[1], S.J. Maxfield[17], D. Meer[39], A. Mehta[17], K. Meier[13], A.B. Meyer[9], H. Meyer[36], J. Meyer[9], V. Michels[9], S. Mikocki[5], I. Milcewicz-Mika[5], D. Milstead[17], D. Mladenov[34], A. Mohamed[17], F. Moreau[28], A. Morozov[7], J.V. Morris[4], M.U. Mozer[12], K. Müller[40], P. Murín[15,43], K. Nankov[34], B. Naroska[10], Th. Naumann[38], P.R. Newman[2], C. Niebuhr[9], A. Nikiforov[26], G. Nowak[5], M. Nozicka[32], R. Oganezov[37], B. Olivier[26], J.E. Olsson[9], S. Osman[19], D. Ozerov[24], V. Palichik[7], I. Panagoulias[9], T. Papadopoulou[9], C. Pascaud[27], G.D. Patel[17], H. Peng[9], E. Perez[8], D. Perez-Astudillo[22], A. Perieanu[9], A. Petrukhin[24], D. Pitzl[9], R. Plačakytė[26], B. Portheault[27], B. Povh[11], P. Prideaux[17], A.J. Rahmat[17], N. Raicevic[30], P. Reimer[31], A. Rimmer[17], C. Risler[9], E. Rizvi[18], P. Robmann[40], B. Roland[3], R. Roosen[3], A. Rostovtsev[24], Z. Rurikova[26], S. Rusakov[25], F. Salvaire[10], D.P.C. Sankey[4], E. Sauvan[21], S. Schätzel[9], S. Schmidt[9], S. Schmitt[9], C. Schmitz[40], L. Schoeffel[8], A. Schöning[39], H.-C. Schultz-Coulon[13], K. Sedlák[31], F. Sefkow[9], R.N. Shaw-West[2], I. Sheviakov[25], L.N. Shtarkov[25], T. Sloan[16], P. Smirnov[25], Y. Soloviev[25], D. South[9], V. Spaskov[7], A. Specka[28], M. Steder[10], B. Stella[33], J. Stiewe[13], I. Strauch[9], U. Straumann[40], D. Sunar[3], V. Tchoulakov[7], G. Thompson[18], P.D. Thompson[2], F. Tomasz[15], D. Traynor[18], P. Truöl[40], I. Tsakov[34], G. Tsipolitis[9,41], I. Tsurin[9], J. Turnau[5], E. Tzamariudaki[26], K. Urban[13], M. Urban[40], A. Usik[25], D. Utkin[24], A. Valkárová[32], C. Vallée[21], P. Van Mechelen[3], A. Vargas Trevino[6], Y. Vazdik[25], C. Veelken[17],

1

S. Vinokurova[9], V. Volchinski[37], K. Wacker[6], J. Wagner[9], G. Weber[10], R. Weber[39], D. Wegener[6], C. Werner[12], M. Wessels[9], B. Wessling[9], C. Wigmore[2], Ch. Wissing[6], R. Wolf[12], E. Wünsch[9], S. Xella[40], W. Yan[9], V. Yeganov[37], J. Žáček[32], J. Zálešák[31], Z. Zhang[27], A. Zhelezov[24], A. Zhokin[24], Y.C. Zhu[9], J. Zimmermann[26], T. Zimmermann[39], H. Zohrabyan[37], and F. Zomer[27]

[1] *I. Physikalisches Institut der RWTH, Aachen, Germany[a]*
[2] *School of Physics and Astronomy, University of Birmingham, Birmingham, UK[b]*
[3] *Inter-University Institute for High Energies ULB-VUB, Brussels; Universiteit Antwerpen, Antwerpen; Belgium[c]*
[4] *Rutherford Appleton Laboratory, Chilton, Didcot, UK[b]*
[5] *Institute for Nuclear Physics, Cracow, Poland[d]*
[6] *Institut für Physik, Universität Dortmund, Dortmund, Germany[a]*
[7] *Joint Institute for Nuclear Research, Dubna, Russia*
[8] *CEA, DSM/DAPNIA, CE-Saclay, Gif-sur-Yvette, France*
[9] *DESY, Hamburg, Germany*
[10] *Institut für Experimentalphysik, Universität Hamburg, Hamburg, Germany[a]*
[11] *Max-Planck-Institut für Kernphysik, Heidelberg, Germany*
[12] *Physikalisches Institut, Universität Heidelberg, Heidelberg, Germany[a]*
[13] *Kirchhoff-Institut für Physik, Universität Heidelberg, Heidelberg, Germany[a]*
[14] *Institut für Experimentelle und Angewandte Physik, Universität Kiel, Kiel, Germany*
[15] *Institute of Experimental Physics, Slovak Academy of Sciences, Košice, Slovak Republic[f]*
[16] *Department of Physics, University of Lancaster, Lancaster, UK[b]*
[17] *Department of Physics, University of Liverpool, Liverpool, UK[b]*
[18] *Queen Mary and Westfield College, London, UK[b]*
[19] *Physics Department, University of Lund, Lund, Sweden[g]*
[20] *Physics Department, University of Manchester, Manchester, UK[b]*
[21] *CPPM, CNRS/IN2P3 - Univ. Mediterranee, Marseille - France*
[22] *Departamento de Fisica Aplicada, CINVESTAV, Mérida, Yucatán, México[k]*
[23] *Departamento de Fisica, CINVESTAV, México[k]*
[24] *Institute for Theoretical and Experimental Physics, Moscow, Russia[l]*
[25] *Lebedev Physical Institute, Moscow, Russia[e]*
[26] *Max-Planck-Institut für Physik, München, Germany*
[27] *LAL, Université de Paris-Sud, IN2P3-CNRS, Orsay, France*
[28] *LLR, Ecole Polytechnique, IN2P3-CNRS, Palaiseau, France*
[29] *LPNHE, Universités Paris VI and VII, IN2P3-CNRS, Paris, France*
[30] *Faculty of Science, University of Montenegro, Podgorica, Serbia and Montenegro[e]*
[31] *Institute of Physics, Academy of Sciences of the Czech Republic, Praha, Czech Republic[i]*
[32] *Faculty of Mathematics and Physics, Charles University, Praha, Czech Republic[i]*
[33] *Dipartimento di Fisica Università di Roma Tre and INFN Roma 3, Roma, Italy*
[34] *Institute for Nuclear Research and Nuclear Energy, Sofia, Bulgaria[e]*
[35] *Paul Scherrer Institut, Villigen, Switzerland*
[36] *Fachbereich C, Universität Wuppertal, Wuppertal, Germany*
[37] *Yerevan Physics Institute, Yerevan, Armenia*
[38] *DESY, Zeuthen, Germany*
[39] *Institut für Teilchenphysik, ETH, Zürich, Switzerland[j]*

[40] *Physik-Institut der Universität Zürich, Zürich, Switzerland[j]*

[41] *Also at Physics Department, National Technical University, Zografou Campus, GR-15773 Athens, Greece*
[42] *Also at Rechenzentrum, Universität Wuppertal, Wuppertal, Germany*
[43] *Also at University of P.J. Šafárik, Košice, Slovak Republic*
[44] *Also at CERN, Geneva, Switzerland*
[45] *Also at Max-Planck-Institut für Physik, München, Germany*
[46] *Also at Comenius University, Bratislava, Slovak Republic*

1   Introduction

At HERA the largest cross section is due to photoproduction, where the beam lepton interacts with the proton via the exchange of a photon at small virtualities $Q^2 \approx 0$. The photoproduction of dijets with high transverse momenta can be calculated within perturbative Quantum Chromodynamics (pQCD) where the transverse momentum of jets provides the hard scale.

Two contributions to the jet cross section can be distinguished: *direct processes* in which the photon itself enters the hard subprocess and *resolved processes* in which the photon fluctuates into partons of which one participates in the hard scatter. The hadronic structure of the proton and photon are described by their respective parton density functions (PDFs).

Measurements of the parton densities of the photon and proton have been performed in several processes in e^+e^-, ep and $p\bar{p}$ collisions. The quark densities in the photon have been determined at e^+e^- colliders. The parton densities of the proton are mainly determined from deep inelastic scattering (DIS) experiments. Drell-Yan and $p\bar{p}$ jet data provide constraints on the gluon density at high longitudinal proton momentum fraction (x_p). Previous dijet data in photoproduction [1], as well as in electroproduction, are shown to constrain the gluon density in the medium x_p region [2, 3]. Compared to e^+e^- data the photoproduction of jets reaches higher scales and is directly sensitive to the gluon density in the photon.

To test predictions of perturbative calculations and current PDF parametrisations this paper investigates dijet production at very small Q^2 in positron proton interactions using the H1 detector at HERA. The transverse momentum (E_t) of the leading jet ranges between 25 and 80 GeV. The range of the photon momentum fraction carried by the parton participating in the hard interaction is $0.1 < x_\gamma < 1.0$. The proton momentum fraction carried by the interacting parton from the proton side is in the range of $0.05 < x_p < 0.7$.

This paper, compared to a previous publication [4], presents new measurements with increased statistical precision and an improved understanding of the systematic uncertainties. In addition, new measurements are made which examine cross sections with different jet topologies. The dijet cross sections are compared with Monte Carlo simulations based on leading order (LO) QCD and parton showers and with next-to-leading order (NLO) pQCD calculations with hadronisation corrections.

2   H1 Detector

The H1 detector is described in detail elsewhere [5]. The detector elements important for this analysis are described below.

The liquid argon (LAr) calorimeter covers a range in polar angle[1] of $4° < \theta < 153°$. The angular region $153° < \theta < 177°$ is covered by the SpaCal (a lead scintillating fibre Spaghetti Calorimeter). The central tracking detector consists of two concentric drift chambers supplemented by two z-drift chambers and has an angular coverage of $25° < \theta < 155°$. These detectors are immersed in a 1.15 T magnetic field.

---

[1]H1 uses a right-handed coordinate system with the z-axis along the direction of the outgoing proton beam. The polar angle θ is defined with respect to the z-axis.

The LAr and SpaCal calorimeters are used to trigger events and to reject non photoproduction events which have an identified scattered positron. Together with the central tracking chambers they provide a measurement of the hadronic final state energies from which jets are reconstructed. The central tracking chambers are also used to reconstruct the event vertex.

The luminosity determination is based on the measurement of the Bethe-Heitler process ($ep \rightarrow ep\gamma$), where the photon is detected in a calorimeter located downstream of the interaction point in the positron beam direction.

3   Event Selection

The data used in this analysis were taken in the years 1999-2000 where positrons of energy $27.6\,\mathrm{GeV}$ were collided with protons of $920\,\mathrm{GeV}$, yielding a centre-of-mass energy of $318\,\mathrm{GeV}$. This sample corresponds to a total integrated luminosity of 66.6 pb^{-1}.

Events were triggered by requiring a combination of sub-triggers utilising different energy thresholds in the LAr calorimeters with additional vertex and timing conditions. The trigger efficiency is above 98% for the event selection used in this analysis.

The event vertex is required to be reconstructed within ±35 cm in z of the nominal interaction point. This ensures that the event can be properly reconstructed and helps to remove proton beam-gas background events. Several topological background finder algorithms are used to remove cosmic muon events. Events with a large missing transverse momentum of more than $20\,\mathrm{GeV}$ are rejected, reducing charged current and any remaining non-ep background to below the 1% level.

Photoproduction events are selected by demanding that there be no scattered positron candidate in the LAr or SpaCal calorimeter, restricting the negative four-momentum transfer squared Q^2 to be below $1\,\mathrm{GeV}^2$. The main source of background comes from neutral current (NC) DIS events in which the scattered positron is misidentified as part of the hadronic final state. These events are suppressed by requiring the inelasticity y to be less than 0.9, where y is reconstructed from the hadronic final state[2]. The phase space is further restricted to $y > 0.1$. Additional restrictions based on the topology of the jet showers [6] are applied that help to reduce the overall DIS background to below 2%. The remaining DIS background is subtracted statistically based on predictions from Monte Carlo simulations.

Jets are reconstructed in the laboratory frame using the inclusive $k_{\perp}$ algorithm [7]. The p_{t}-weighted recombination scheme is used in which the jets are considered massless and the separation parameter is set to 1. The jets are required to be contained in the LAr calorimeter by the restriction that $-0.5 < \eta_{\mathrm{jet}} < 2.75$, where the pseudo-rapidity is given by $\eta = -\ln\tan\theta/2$. Only the two highest E_{t} jets in the chosen η range are considered. Asymmetric cuts on the jets E_{t} are applied to avoid regions of phase space where the existing NLO QCD calculations suffer from an incomplete cancellation of infrared singularities. The leading jet is required to have $E_{\mathrm{t,max}} > 25\,\mathrm{GeV}$ and the other jet $E_{\mathrm{t,2nd}} > 15\,\mathrm{GeV}$. The total number of selected events within the phase space summarised in table 1 is about $14,000$.

---

[2]The inclusion of the scattered positron into the hadronic final state causes y to be reconstructed at values close to one.

$$Q^2 < 1\,\mathrm{GeV}^2$$
$$0.1 < y < 0.9$$
$$E_{\mathrm{t,max}} > 25\,\mathrm{GeV}$$
$$E_{\mathrm{t,2nd}} > 15\,\mathrm{GeV}$$
$$-0.5 < \eta_{\mathrm{jet}} < 2.75$$

Table 1: Definition of the phase space of the dijet cross section measurements.

4   Jet Observables

This analysis studies the dijet cross section as a function of the two observables x_γ and x_p and as a function of the angle of the dijets in their centre-of-mass system, $|\cos\theta^*|$. These variables are reconstructed as follows:

$$x_\gamma = \frac{1}{2yE_e} \cdot \sum_{i=1}^{2} E_{\mathrm{t,i}} \cdot e^{-\eta_i} \tag{1}$$

$$x_p = \frac{1}{2E_p} \cdot \sum_{i=1}^{2} E_{\mathrm{t,i}} \cdot e^{+\eta_i} \tag{2}$$

$$|\cos\theta^*| = |\tanh(\eta_1 - \eta_2)/2|\,. \tag{3}$$

Here E_e and E_p are the energies of the positron and proton beam, respectively. $E_{\mathrm{t,1}}$ and $E_{\mathrm{t,2}}$ are the transverse energies of the two jets and η_1 and η_2 their pseudorapidities. In the leading order picture x_γ and x_p represent, respectively, the longitudinal photon and proton momentum fractions entering the hard interaction.

5   QCD Models

The PYTHIA [8] Monte Carlo program contains Born level QCD matrix elements of direct and resolved hard processes. Higher order QCD radiation is represented by parton showers in the leading logarithm approximation. PYTHIA uses the Lund string model for hadronisation. Here version 6.1 of PYTHIA is used with the leading order parametrisation CTEQ5L [9] for the proton PDFs and GRV-LO [10] for the photon PDFs. The PYTHIA predictions need to be scaled up by a factor of 1.2 to describe the dijet data, this factor accounting for missing higher orders in the PYTHIA calculation.

The HERWIG [11] Monte Carlo, which uses the cluster model for hadronisation, is found to produce similar results to PYTHIA, but a scale factor of 1.55 is required to reproduce the total dijet cross section.

Parton level NLO QCD dijet cross sections are obtained using a program [12] based on the subtraction method [13] for the cancellation of infrared singularities. In the calculation of the NLO cross sections a two-loop α_s is taken and the parametrisation CTEQ6M [14] is chosen. Using instead the MRST2001 [15] PDFs similar results are found. The uncertainty of the NLO QCD predictions due to the choice of the proton PDFs is calculated from the 40 eigenvectors of the CTEQ6M PDFs. It varies from 4% at low x_p to 20% at high x_p. For the photon PDFs the GRV-HO [16] parametrisation is used. Using instead the AFG-HO [17] photon PDFs, differences of the order of 20% in the resolved enhanced region and of 10% in the direct enhanced region are seen [6].

The renormalisation scale μ_r and the factorisation scale μ_f are set to the sum of the transverse momenta of the outgoing partons divided by two, on an event-by-event basis. The effect of the choice of scale was studied by varying the common scale $\mu = \mu_r = \mu_f$ by a factor two up and one half down. The uncertainty on the NLO QCD predictions arising from this procedure is found to vary between a few percent and almost $\pm 30\%$. The uncertainty from the PDFs is in general much smaller than the error from the scale uncertainty, except at large x_p where it grows to be about twice as big.

The NLO QCD predictions are compared to the data after a correction for hadronisation effects. The correction δ_{had} is determined from the Monte Carlo models and varies between 1% and 6%. It is defined as the ratio of the cross sections calculated with jets reconstructed from hadrons to those from partons (after the parton shower). HERWIG and PYTHIA are used to calculate a mean correction factor applied to the NLO QCD predictions. Its uncertainty is taken as half the difference between the HERWIG and PYTHIA results. This uncertainty (3 - 6%) is in general smaller than the dominant theory uncertainty which depending on phase space is given by the scale or PDF uncertainty.

6   Data Correction

The data are corrected for detector effects (resolution and efficiencies) using Monte Carlo event samples. The correction factors are calculated from the ratio of the cross sections with jets reconstructed from hadrons (hadron level) and from detector objects (detector level). The correction is applied bin-by-bin. The bin sizes used in the cross section measurements are matched to the resolution and generally result in high acceptance and purity[3], typically above 60%, with a minimum requirement of 30%. The Monte Carlo events are reweighted to take into account the imperfect description of the observed y and $|\cos\theta^*|$ distributions. Both HERWIG and PYTHIA produce similar correction factors and a mean correction factor is used. The uncertainty in the correction factor is taken as half the difference between HERWIG and PYTHIA. Half the difference between the reweighted and unweighted results is taken as an additional uncertainty.

---

[3]The acceptance (purity) is defined as the ratio of the number of events generated in a bin which are reconstructed in that bin to the total number of events generated (reconstructed) in that bin.

7 Systematic Uncertainties

For the jet cross sections the following sources of correlated and uncorrelated systematic errors are considered.

- The LAr hadronic energy scale is known to within 1.5%. It is estimated from the p_t balance of the scattered positron with the hadronic final state in DIS and from the p_t balance of dijet events in photoproduction in the p_t range of this analysis. The resulting correlated uncertainties on the cross section are typically 7% at low x_p and 15% at high x_p.

- The SpaCal hadronic energy scale is known to better than 8%, resulting in correlated uncertainties of typically 1% to 2%.

- The total uncertainty in the data correction factor (see section 6) results in a typical error of 2% to 7% and is considered as uncorrelated.

- The trigger efficiency uncertainty results in an uncorrelated error of 2%.

- The subtraction of the DIS background leads to an uncorrelated error of less than 1%.

- The uncertainty in the luminosity measurement leads to an overall normalisation error of 1.5%.

8 Results

The dijet cross section as a function of $|\cos\theta^*|$ is shown in figure 1 and listed in table 2. This distribution is sensitive to the dynamics of the hard interaction. The measurement is presented for the direct ($x_\gamma > 0.8$) and resolved ($x_\gamma < 0.8$) enriched samples separately. The cross section shows no enhancement in the region of large $|\cos\theta^*|$ because the cuts on the jet transverse momenta suppress the phase space in this region. This phase space suppression is less prominent for large energies in the centre-of-mass of the hard subprocess. Requiring in addition that the dijet mass M_{JJ} be above $65\,\text{GeV}$, the shape of the measured cross section is changed towards that expected from the QCD matrix elements. The cross section in the resolved sample rises more rapidly with $|\cos\theta^*|$ than that in the direct sample due to the dominating gluon propagator in resolved processes [1,4].

Figure 2 (table 3) shows the cross section as a function of x_γ in two regions of x_p. For $x_p < 0.1$ the fraction of events induced by gluons from the proton side is estimated to be about 70%. It decreases to 15% at the highest x_p reached in this analysis. Thus the two regions roughly distinguish between photon-gluon fusion ($x_p < 0.1$) and photon-quark scattering ($x_p > 0.1$). Over the entire range in x_γ and in both x_p regions the NLO QCD predictions agree with the data within uncertainties. The leading order Monte Carlo predictions also describe the data.

The cross section as a function of x_p is depicted in figure 3. Here the measurement is made in two regions of x_γ ($x_\gamma > 0.8$ and $x_\gamma < 0.8$). In both regions the agreement of the NLO

8

QCD predictions with the data is within 10% at low x_p. This is covered by the experimental uncertainties which are dominated by the hadronic energy scale uncertainty. The two other significant contributions to the experimental uncertainty are the model uncertainty (5% at low x_p) and the statistical uncertainty ($\approx 20\%$ in the highest x_p bin).

Since the pseudorapidities of the two jets are sensitive to the momentum distributions of the interacting partons, the cross sections as a function of x_p (figure 4, table 4) and of $E_{\mathrm{t,max}}$ (figure 5, table 5) are measured for three different topologies of the final state: the case where both jets are in the "backward" direction ($\eta_{1,2} < 1$), where both jets are in the "forward" direction ($\eta_{1,2} > 1$), and where one jet is in the "forward" ($\eta_i > 1$) direction and one is in the "backward" ($\eta_j < 1$) direction. As before, the measurement is performed separately in two regions of x_γ. The NLO QCD predictions describe the data in x_p and $E_{\mathrm{t,max}}$ well, except for large x_p in the direct enhanced sample and with both jets going forward.

9   Conclusion

In this paper a new and more precise measurement of high E_{t} dijet photoproduction is presented. Differential cross sections are measured in two regions of the observable x_γ. They are studied as a function of $|\cos\theta^*|$ and x_p. Furthermore the cross sections as a function of $E_{\mathrm{t,max}}$ and x_p are investigated for different jet topologies. Both the NLO QCD calculation and the PYTHIA Monte Carlo simulation provide a reasonable description of the data.

The region of $x_\gamma > 0.8$ (direct photon enhanced region), in which the photon predominantly interacts directly with the proton, is particularly well suited to test proton structure as the photon structure plays no significant role there. At high $E_{\mathrm{t,max}}$ and large x_p the dominant theoretical uncertainty comes from the uncertainty of the proton parton density functions. The data in the region of $x_\gamma < 0.8$ (resolved photon enhanced region), where the photon mainly behaves like a hadronic object, may also provide additional constraints on the photon parton density functions.

Acknowledgements

References

[1] S. Chekanov *et al.* [ZEUS Collaboration], Eur. Phys. J. C **23** (2002) 4 [hep-ex/0112029].

[2] S. Chekanov *et al.* [ZEUS Collaboration], Eur. Phys. J. C **42** (2005) 1 [hep-ph/0503274].

[3] C. Adloff *et al.* [H1 Collaboration], Eur. Phys. J. C **19** (2001) 289 [hep-ex/0010054].

[4] C. Adloff *et al.* [H1 Collaboration], Eur. Phys. J. C **25** (2002) 13 [hep-ex/0201006].

[5] I. Abt. *et al* [H1 Collaboration], Nucl. Instrum. Meth. A **386** (1997) 310;
    I. Abt. *et al* [H1 Collaboration], Nucl. Instrum. Meth. A **386** (1997) 348.

[6] I. Strauch, "Jets with high Transverse Momenta in Photoproduction at HERA", PhD Thesis, Univ. Hamburg, 2004, available at http://www-h1.desy.de/publications/theses_list.html.

[7] S. Catani, Y. L. Dokshitzer, M. H. Seymour and B. R. Webber, Nucl. Phys. B **406** (1993) 187.

[8] T. Sjöstrand, Comput. Phys. Commun. **82** (1994) 74;
    T. Sjöstrand *et al.*, Comput. Phys. Commun. **135** (2001) 238 [hep-ph/0010017].

[9] H.L. Lai *et al.* [CTEQ Collaboration], Eur. Phys. J. C **12** (2000) 375 [hep-ph/9903282].

[10] M. Glück, E. Reya and A. Vogt, Phys. Rev. D **46** (1992) 1973.

[11] G. Marchesini *et al.*, Comput. Phys. Commun. **67** (1992) 465;
     G. Corcella *et al.*, "HERWIG 6.4 release note" [hep-ph/0201201].

[12] S. Frixione, Nucl. Phys. B **507** (1997) 295 [hep-ph/9706545];
     S. Frixione and G. Ridolfi, Nucl. Phys. B **507** (1997) 315 [hep-ph/9707345].

[13] Z. Kunszt and D. E. Soper, Phys. Rev. D **46** (1992) 192.

[14] J. Pumplin *et al.*, JHEP. **7** (2002) 12 [hep-ph/0201195].

[15] A. D. Martin, R. G. Roberts, W. J. Stirling and R. S. Thorne, Eur. Phys. J. C **23** (2002) 73 [hep-ph/0110215].

[16] M. Glück, E. Reya and A. Vogt, Phys. Rev. D **46** (1992) 1973.

[17] P. Aurenche, J. P. Guillet and M. Fontannaz, Z. Phys. C **64** (1994) 621 [hep-ph/9406382].

Figure 1: Bin averaged cross sections as a function of $|\cos\theta^*|$ for data (points), NLO QCD calculations with (solid line) and without (dashed line) hadronisation corrections δ_{had} and for the PYTHIA Monte Carlo predictions (dotted line) scaled by a factor of 1.2. The inner bars indicate the statistical uncertainty and the outer error bars show the statistical and systematic errors added in quadrature. The inner (hatched) band of the NLO$\times(1+\delta_{\mathrm{had}})$ result is the scale uncertainty, the outer (shaded) band is the total uncertainty. The cross sections are shown for two regions in x_γ enhancing the resolved (left) or direct (right) photon contribution, with and without an additional cut applied on the invariant dijet mass (M_{JJ}).

11

Figure 2: Bin averaged cross sections as a function of x_γ for data (points), NLO QCD calculations with (solid line) and without (dashed line) hadronisation corrections δ_{had} and for the PYTHIA Monte Carlo predictions (dotted line) scaled by a factor of 1.2. The inner bars indicate the statistical uncertainty and the outer error bars show the statistical and systematic errors added in quadrature. The inner (hatched) band of the NLO$\times(1+\delta_{\mathrm{had}})$ result is the scale uncertainty, the outer (shaded) band is the total uncertainty. The cross sections are shown separately for two regions in x_p.
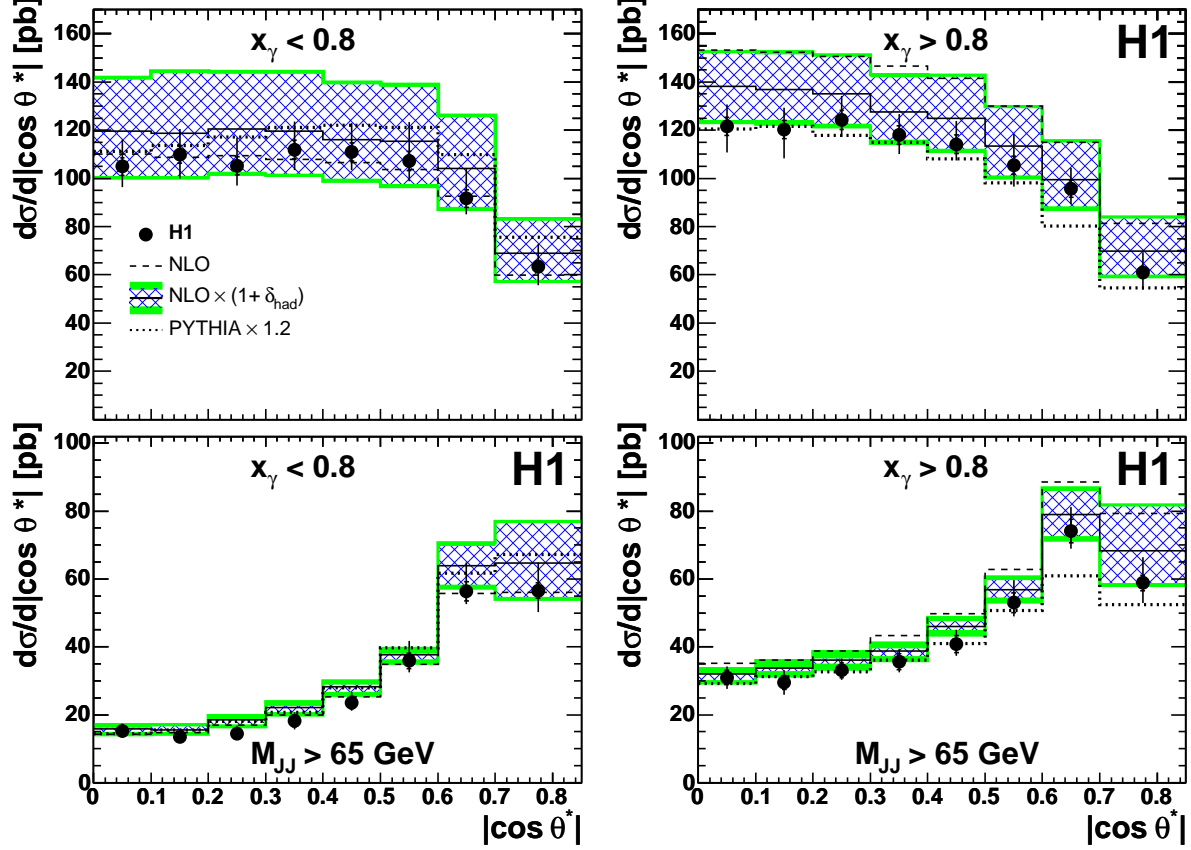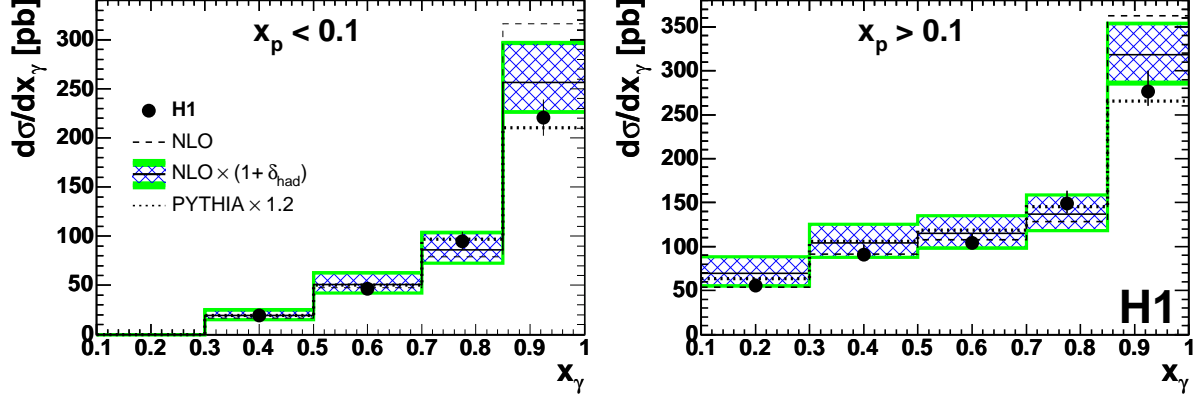

Figure 3: Bin averaged cross sections as a function of x_p for data (points), NLO QCD predictions with (solid line) and without (dashed line) hadronisation corrections δ_{had} and for the PYTHIA Monte Carlo predictions (dotted line) scaled by a factor of 1.2. The inner bars indicate the statistical uncertainty and the outer error bars show the statistical and systematic errors added in quadrature. The inner (hatched) band of the NLO$\times(1+\delta_{\mathrm{had}})$ result is the scale uncertainty, the outer (shaded) band is the total uncertainty. The cross sections are shown separately for two regions in x_γ enhancing the resolved (left) or direct (right) photon contribution.

12

Figure 4: Bin averaged cross sections as a function of x_p with different topologies of jet η for data (points), NLO QCD calculations with (solid line) and without (dashed line) hadronisation corrections δ_{had} and for the PYTHIA Monte Carlo predictions (dotted line) scaled by a factor of 1.2. The inner bars indicate the statistical uncertainty and the outer error bars show the statistical and systematic errors added in quadrature. The inner (hatched) band of the NLO$\times(1 + \delta_{had})$ result is the scale uncertainty, the outer (shaded) band is the total uncertainty. Th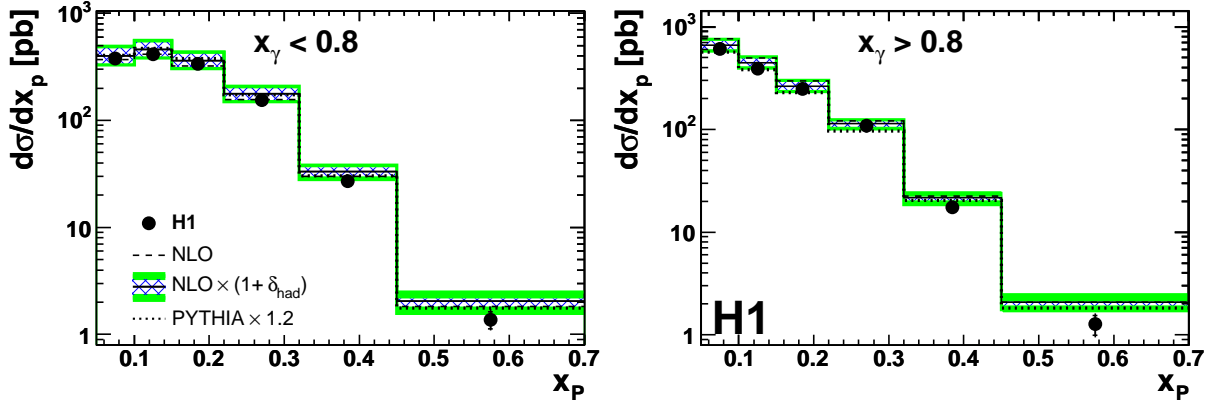e cross sections are shown separately for two regions in x_γ enhancing the resolved (left) or direct (right) photon contribution.

13

Figure 5: Bin averaged cross sections as a function of $E_{\text{t,max}}$ with different topologies of jet η for data (points), NLO QCD calculations with (solid line) and without (dashed line) hadronisation corrections δ_{had} and for the PYTHIA Monte Carlo predictions (dotted line) scaled by a factor of 1.2. The inner bars indicate the statistical uncertainty and the outer error bars show the statistical and systematic errors added in quadrature. The inner (hatched) band of the NLO$\times(1 + \delta_{\text{had}})$ result is the scale uncertainty, the outer (shaded) band is the total uncertainty. The cross sections are shown separately for two regions in x_γ enhancing the resolved (left) or direct (right) photon contribution.
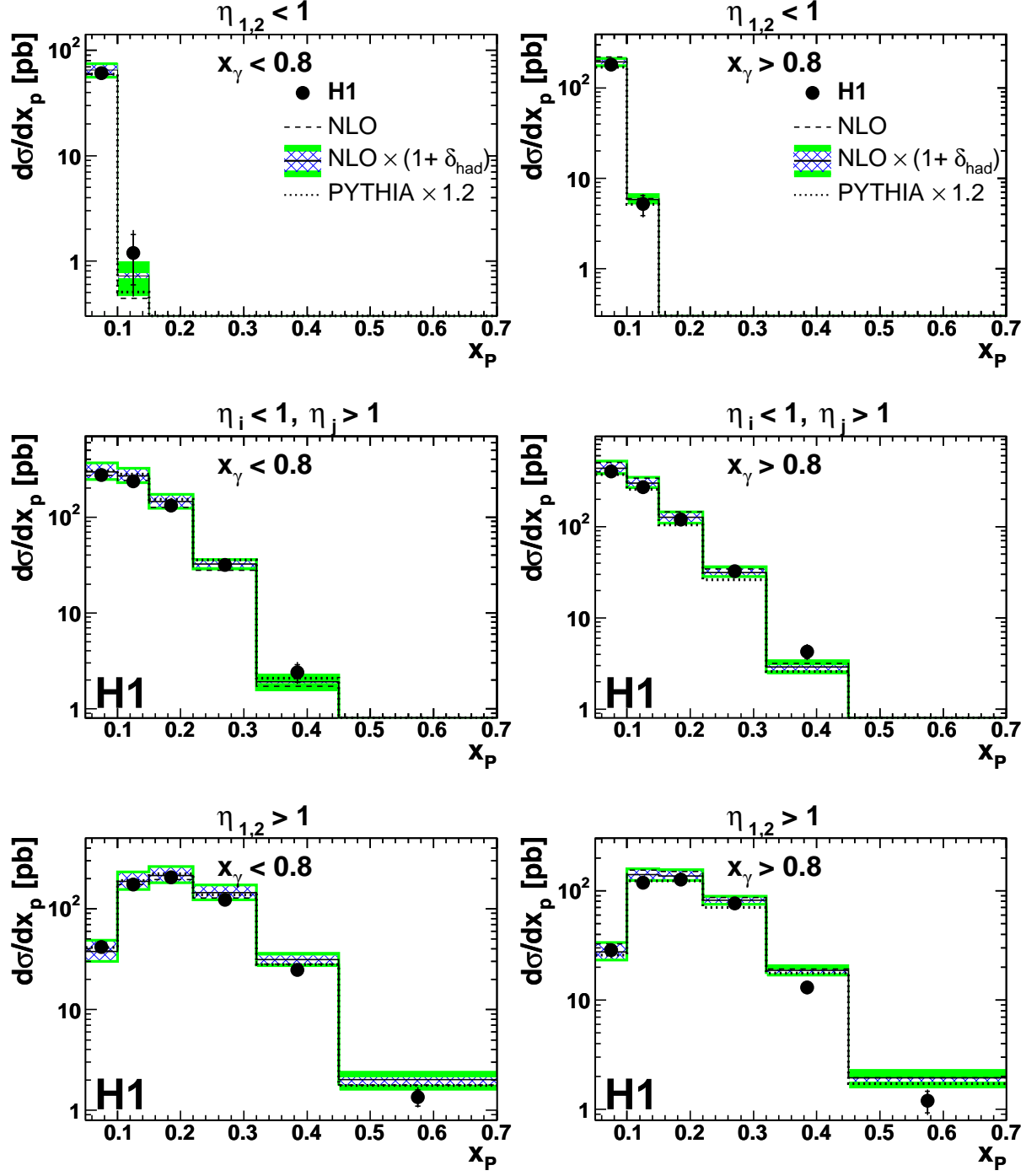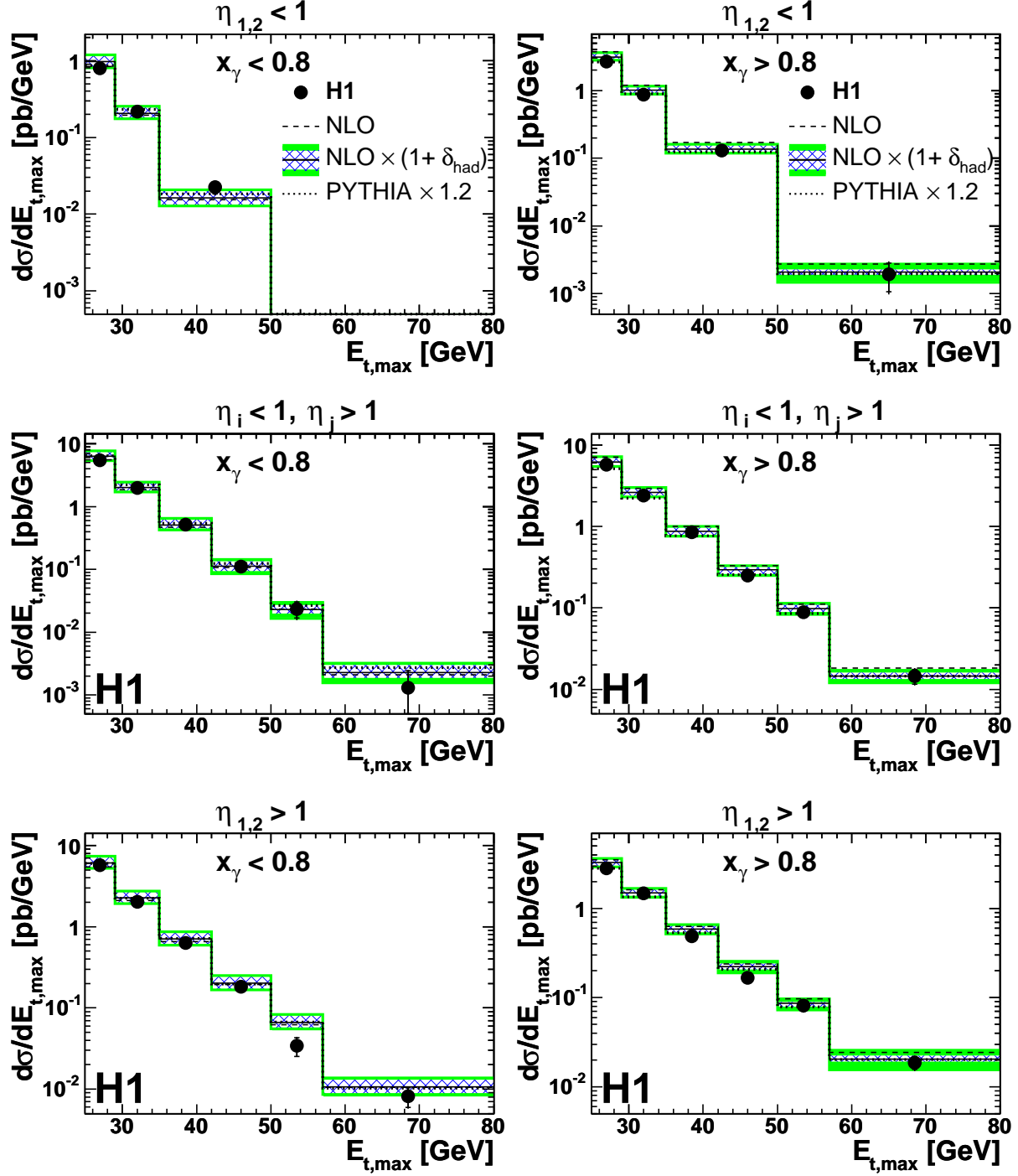
14

$\lvert \cos\theta^* \rvert$	$\frac{d\sigma}{d\lvert\cos\theta^*\rvert}$ [pb]	δ_{stat} [%]	δ_{tot} [%]	δ_{LAr} [%]	δ_{mod} [%]
		$x_\gamma < 0.8$			
0.00-0.10	104.9	3.4	10.7/8.1	9.6/5.0	1.5/2.8
0.10-0.20	110.0	3.3	9.6/9.2	8.3/5.5	2.1/3.6
0.20-0.30	105.2	3.5	11.1/7.7	9.4/5.7	3.1/3.1
0.30-0.40	111.9	3.5	10.5/7.5	9.1/6.1	1.8/1.6
0.40-0.50	111.0	3.5	10.8/6.8	9.5/5.2	1.8/1.6
0.50-0.60	107.2	3.7	15.2/7.8	10.2/5.6	5.8/3.5
0.60-0.70	91.65	3.9	14.0/7.0	10.2/4.6	4.8/3.0
0.70-0.85	63.34	3.8	14.9/12.2	9.2/5.8	10.0/9.9
		$x_\gamma > 0.8$			
0.00-0.10	121.6	3.1	7.5/9.0	6.3/5.0	1.3/3.4
0.10-0.20	120.3	3.1	7.4/10.0	6.3/5.6	1.3/3.9
0.20-0.30	124.3	3.1	8.0/5.7	6.9/3.5	1.3/1.7
0.30-0.40	118.0	3.3	7.4/6.7	5.8/5.1	2.2/2.2
0.40-0.50	114.2	3.4	8.5/6.0	7.2/4.2	1.4/1.4
0.50-0.60	105.4	3.6	12.4/8.3	7.9/4.6	6.3/5.5
0.60-0.70	95.70	3.8	9.1/6.8	6.7/4.7	2.9/2.3
0.70-0.85	60.91	3.7	13.9/11.5	8.6/4.3	9.8/9.8
		$x_\gamma < 0.8$ and $M_{\mathrm{JJ}} > 65\,\mathrm{GeV}$			
0.00-0.10	15.19	9.4	14.7/12.3	9.8/5.1	3.6/4.1
0.10-0.20	13.51	9.8	15.7/12.8	11.1/5.4	3.5/4.2
0.20-0.30	14.38	10.1	16.3/11.2	11.1/3.1	3.3/3.3
0.30-0.40	18.15	9.0	13.8/13.3	8.2/8.2	5.1/4.9
0.40-0.50	23.61	7.8	13.3/10.3	9.2/5.8	3.0/2.7
0.50-0.60	35.90	6.5	16.5/9.6	10.7/6.4	5.5/2.2
0.60-0.70	56.38	5.1	15.1/6.8	10.9/3.4	4.5/2.2
0.70-0.85	56.58	4.0	14.6/11.3	9.0/4.7	9.4/9.2
		$x_\gamma > 0.8$ and $M_{\mathrm{JJ}} > 65\,\mathrm{GeV}$			
0.00-0.10	30.99	6.7	10.4/11.0	7.1/6.0	2.6/3.8
0.10-0.20	29.54	6.9	12.2/12.1	8.4/5.4	5.1/6.0
0.20-0.30	33.16	6.7	10.3/8.8	7.1/4.5	2.5/2.6
0.30-0.40	35.60	6.6	10.5/8.7	7.1/4.8	2.4/2.3
0.40-0.50	40.79	6.2	10.4/8.2	7.6/4.4	2.2/2.2
0.50-0.60	53.04	5.5	12.4/7.6	7.8/4.4	4.0/2.0
0.60-0.70	74.15	4.6	9.4/7.0	6.8/4.4	2.7/1.9
0.70-0.85	58.86	3.9	12.8/10.1	8.6/4.1	8.1/8.1

Table 2: Bin averaged cross sections for dijet photoproduction in intervals of $\lvert\cos\theta^*\rvert$ shown with the statistical error (δ_{stat}), the total error including statistical and systematic errors (δ_{tot}), the error coming from the LAr hadronic energy scale uncertainty (δ_{LAr}) and the error from the model uncertainty and the Monte Carlo reweighting (δ_{mod}). Two numbers are shown to allow for asymmetric errors ($+/-$).

x_γ	$\frac{d\sigma}{dx_\gamma}$ [pb]	δ_{stat} [%]	δ_{tot} [%]	δ_{LAr} [%]	δ_{mod} [%]
	$x_p < 0.1$				
0.30-0.50	19.11	5.8	11.9/10.4	7.4/7.0	4.6/3.4
0.50-0.70	46.43	3.5	12.0/10.3	7.1/5.9	7.6/7.2
0.70-0.85	94.58	2.9	10.3/9.1	6.9/5.7	6.6/6.2
0.85-1.00	220.7	1.8	8.4/8.5	5.4/5.5	5.8/5.8
	$x_p > 0.1$				
0.10-0.30	55.51	4.0	14.1/8.0	12.3/6.3	2.4/1.7
0.30-0.50	90.88	2.8	12.4/6.4	10.9/4.8	2.7/2.6
0.50-0.70	103.8	2.5	10.9/6.4	9.6/5.0	2.2/2.2
0.70-0.85	148.7	2.4	9.9/7.2	8.9/5.5	2.4/2.7
0.85-1.00	276.5	1.9	8.6/6.0	7.8/3.5	0.7/2.1

Table 3: Bin averaged cross sections for dijet photoproduction in intervals of x_γ shown with the statistical error (δ_{stat}), the total error including statistical and systematic errors (δ_{tot}), the error coming from the LAr hadronic energy scale uncertainty (δ_{LAr}) and the error from the model uncertainty and the Monte Carlo reweighting (δ_{mod}). Two numbers are shown to allow for asymmetric errors ($+/-$).

x_p	$\frac{d\sigma}{dx_p}$ [pb]	δ_{stat} [%]	δ_{tot} [%]	δ_{LAr} [%]	δ_{mod} [%]
		$x_\gamma < 0.8$ and $\eta_{1,2} < 1$			
0.05-0.10	60.60	6.3	11.9/11.8	7.2/7.2	6.1/5.9
0.10-0.15	1.18	50.0	65.2/63.9	30.0/30.0	26.7/25.8
		$x_\gamma < 0.8$ and $\eta_i < 1, \eta_j > 1$			
0.05-0.10	276.2	3.0	10.9/9.0	6.7/6.1	6.1/5.4
0.10-0.15	235.4	3.6	13.1/8.0	9.3/5.2	5.5/4.5
0.15-0.22	132.0	4.0	13.3/8.1	10.3/5.7	4.4/3.6
0.22-0.32	31.80	6.4	16.4/12.0	10.5/4.2	9.2/9.0
0.32-0.45	2.38	20.5	28.1/24.3	14.1/7.7	10.9/10.3
		$x_\gamma < 0.8$ and $\eta_{1,2} > 1$			
0.05-0.10	41.84	6.8	11.4/11.8	8.1/7.1	3.7/4.4
0.10-0.15	175.1	3.9	11.2/8.5	9.5/5.3	3.6/4.0
0.15-0.22	205.5	3.1	10.5/7.3	9.3/5.8	1.4/1.7
0.22-0.32	122.7	3.3	13.7/6.6	12.4/4.4	1.4/2.0
0.32-0.45	24.69	6.1	14.0/10.1	11.8/5.5	2.3/3.4
0.45-0.70	1.35	18.4	25.5/21.1	15.2/5.2	6.4/7.0
		$x_\gamma > 0.8$ and $\eta_{1,2} < 1$			
0.05-0.10	180.5	3.8	8.1/7.8	6.2/5.8	2.9/2.9
0.10-0.15	5.17	25.0	29.4/29.2	12.0/12.0	9.0/8.8
		$x_\gamma > 0.8$ and $\eta_i < 1, \eta_j > 1$			
0.05-0.10	401.9	2.4	8.7/8.4	5.6/5.2	5.8/5.8
0.10-0.15	269.6	3.3	9.0/6.6	7.0/4.0	3.6/3.6
0.15-0.22	120.1	4.0	9.9/7.3	7.8/4.5	3.6/3.6
0.22-0.32	32.43	6.4	12.3/8.5	9.4/4.2	2.8/2.8
0.32-0.45	4.27	16.0	21.3/19.8	10.8/8.2	8.0/7.9
		$x_\gamma > 0.8$ and $\eta_{1,2} > 1$			
0.05-0.10	28.58	7.7	11.2/15.5	6.2/5.5	4.5/7.2
0.10-0.15	118.6	4.5	7.4/11.8	5.2/4.5	1.8/5.1
0.15-0.22	126.7	4.1	10.7/9.8	8.8/2.7	2.1/4.5
0.22-0.32	76.27	4.6	11.9/10.0	9.7/3.2	3.5/5.0
0.32-0.45	13.00	9.3	14.5/12.9	9.5/3.7	3.1/4.8
0.45-0.70	1.20	22.4	27.4/26.2	13.8/8.8	7.1/8.0

Table 4: Bin averaged cross sections for dijet photoproduction in intervals of x_p shown with the statistical error (δ_{stat}), the total error including statistical and systematic errors (δ_{tot}), the error coming from the LAr hadronic energy scale uncertainty (δ_{LAr}) and the error from the model uncertainty and the Monte Carlo reweighting (δ_{mod}). Two numbers are shown to allow for asymmetric errors ($+/-$).

$E_{t,max}$ [GeV]	$\frac{d\sigma}{dE_{t,max}}$ [$\frac{pb}{GeV}$]	δ_{stat} [%]	δ_{tot} [%]	δ_{LAr} [%]	δ_{mod} [%]
	$x_\gamma < 0.8$ and $\eta_{1,2} < 1$				
25-29	0.796	6.1	16.5/14.3	8.5/4.1	12.0/11.8
29-35	0.217	9.2	12.5/13.7	4.5/8.8	4.9/4.0
35-50	0.022	17.8	22.7/21.1	7.4/7.8	8.9/7.7
	$x_\gamma < 0.8$ and $\eta_i < 1, \eta_j > 1$				
25-29	5.500	2.6	11.0/8.0	7.8/5.4	5.4/4.9
29-35	1.989	3.3	13.1/8.3	9.9/5.8	5.3/4.4
35-42	0.517	5.8	15.4/10.7	9.0/5.6	7.8/6.7
42-50	0.110	12.0	20.3/14.9	10.5/5.2	8.3/6.8
50-57	0.023	28.9	36.5/34.0	15.0/15.0	11.6/9.6
57-80	0.001	86.4	92.4/90.4	20.0/20.0	19.1/17.0
	$x_\gamma < 0.8$ and $\eta_{1,2} > 1$				
25-29	5.691	2.6	11.6/6.6	10.7/4.4	1.2/2.1
29-35	2.031	3.0	11.1/8.0	9.9/6.2	1.2/2.0
35-42	0.631	5.2	12.4/8.3	10.7/5.4	2.0/2.3
42-50	0.181	8.9	15.6/12.5	11.2/7.8	3.3/3.4
50-57	0.034	25.7	29.5/27.7	12.5/7.0	6.6/6.6
57-80	0.008	27.0	32.7/29.3	14.8/7.0	8.6/8.4
	$x_\gamma > 0.8$ and $\eta_{1,2} < 1$				
25-29	2.664	3.3	8.8/8.8	5.8/5.8	5.3/5.3
29-35	0.872	4.6	9.6/9.3	5.5/5.2	5.9/5.8
35-50	0.131	7.5	12.0/11.2	6.3/6.5	5.3/4.8
50-80	0.002	44.7	54.2/52.3	21.0/21.0	18.3/17.0
	$x_\gamma > 0.8$ and $\eta_i < 1, \eta_j > 1$				
25-29	5.751	2.4	9.0/7.6	6.4/4.5	5.3/5.3
29-35	2.400	2.9	8.6/7.4	6.5/5.1	4.1/4.1
35-42	0.854	4.6	10.2/7.6	7.5/4.5	3.8/3.5
42-50	0.249	8.2	13.4/10.4	8.2/5.0	4.4/3.5
50-57	0.089	14.5	19.1/16.6	7.9/5.7	6.5/5.4
57-80	0.015	20.3	25.6/23.9	10.0/10.0	8.5/7.1
	$x_\gamma > 0.8$ and $\eta_{1,2} > 1$				
25-29	2.833	3.7	7.9/10.7	6.3/3.5	1.8/4.8
29-35	1.474	3.9	11.0/10.4	9.4/2.5	2.1/4.9
35-42	0.487	6.0	11.7/12.4	8.3/5.1	4.5/6.1
42-50	0.167	9.6	14.0/13.7	8.7/5.4	3.9/5.2
50-57	0.081	14.0	18.3/16.7	10.2/4.7	5.7/6.2
57-80	0.019	16.7	19.8/19.7	8.1/7.6	6.2/6.4

Table 5: Bin averaged cross sections for dijet photoproduction in intervals of $E_{t,max}$ shown with the statistical error (δ_{stat}), the total error including statistical and systematic errors (δ_{tot}), the error coming from the LAr hadronic energy scale uncertainty (δ_{LAr}) and the error from the model uncertainty and the Monte Carlo reweighting (δ_{mod}). Two numbers are shown to allow for asymmetric errors ($+/-$).